

## Restoration of photon indistinguishability in the emission of a semiconductor quantum dot

S. Varoutsis, S. Laurent, P. Kramper, A. Lemaître, I. Sagnes, I. Robert-Philip, and I. Abram  
 CNRS/Laboratoire de Photonique et de Nanostructures, Route de Nozay, 91460 Marcoussis, France

(Received 29 April 2005; published 13 July 2005)

We report on a series of experiments on the second-order interference of two single photons emitted sequentially by a single quantum dot. The visibility of this interference probes the indistinguishability of the emitted photons; visibilities as high as 0.75 at 4 K have been achieved. At higher temperatures, dephasing of the quantum dot exciton degrades the indistinguishability of the emitted photons and the visibility of the interference. However, we demonstrate that engineering of the radiative lifetime of the quantum dot by the implementation of the Purcell effect in a microcavity, can restore indistinguishability and improve the visibility of second-order interference. At the same time, we demonstrate the resonant character of the Purcell effect.

DOI: [10.1103/PhysRevB.72.041303](https://doi.org/10.1103/PhysRevB.72.041303)

PACS number(s): 78.67.Hc, 42.50.Dv, 42.50.Pq, 42.50.St

When two indistinguishable single photons enter separately, but simultaneously, into the two input ports of a beam splitter, they both emerge together, along the same output port of the beam splitter, as if they had “coalesced” into a two-photon Fock state.<sup>1</sup> This second-order interference phenomenon has been used to highlight many fundamental aspects of quantum optics, such as the nonlocality of quantum mechanics,<sup>2</sup> or the measurement of the photon transit time in superluminal photon tunneling.<sup>3</sup> Moreover, the interference of two single photons on a beam splitter plays a central role in recent proposals for the realization of two-qubit gates as key elements of photon-based quantum computing schemes.<sup>4</sup> The two-photon interference phenomenon was first observed using pairs of twin photons produced simultaneously by parametric down conversion.<sup>1</sup> More recently, it was demonstrated using two single photons originating from two distinct emitters: two independent but synchronized optical parametric oscillators,<sup>5</sup> two sequential emission events of a single atom,<sup>6</sup> and a single semiconductor quantum dot<sup>7</sup> excited by a pair of laser pulses.

The situation in which two-photon interference occurs between truly independent photons presents an important difference from that of twin parametric photons. Each individual emitter may be subject to fluctuations independently of the other, thus “marking” each of the two photons differently and destroying their indistinguishability. For the case of a semiconductor quantum dot, for example, such fluctuations are due to the exciton-phonon interaction which causes the dephasing of the emitting exciton state, with a characteristic dephasing time  $T_2^*$ . In order to reduce the impact of dephasing on the emission process, and thus restore the indistinguishability of the emitted photons, the radiative lifetime of the emitter (denoted by  $T_1$ ) must be shortened, so that it dominates over  $T_2^*$  in determining the overall coherence time of the photon wave train,  $T_2$ , defined by

$$\frac{1}{T_2} = \frac{1}{2T_1} + \frac{1}{T_2^*}. \quad (1)$$

This can be achieved by embedding the quantum dot in a microcavity,<sup>8</sup> thus taking advantage of cavity quantum electrodynamics effects (Purcell effect<sup>9</sup>). The spontaneous emis-

sion rate of a dipole  $\mu$  is given by Fermi’s Golden Rule as

$$\frac{1}{T_1} = \frac{2\pi}{\hbar} |\mu \cdot E_{vac}(r)|^2 \rho(\hbar\omega), \quad (2)$$

where  $E_{vac}(r)$  is the vacuum electric field at  $r$ , the site of the emitting dipole, while  $\rho(\hbar\omega)$  is the density of electromagnetic modes at the emission frequency  $\omega$ . In the vicinity of an isolated cavity mode with Lorentzian spectrum of width  $\gamma$  and central frequency  $\Omega$ , the density of states can be written as

$$\rho(\hbar\omega) = \frac{\hbar\gamma/\pi}{(\hbar\omega - \hbar\Omega)^2 + (\hbar\gamma)^2}, \quad (3)$$

underscoring the importance of the resonance condition in enhancing spontaneous emission. The idea of exploiting the Purcell effect has been successfully implemented by Santori *et al.*,<sup>7</sup> who reported the observation of two-photon interference with photons obtained from a semiconductor quantum dot and opened the way to the use of quantum dots as sources of indistinguishable photons for quantum optics, such as the observation of entanglement.<sup>10</sup>

In this paper, by studying the visibility of the interference of two photons emitted sequentially by a single quantum dot embedded in a micropillar microcavity as a function of temperature, we demonstrate that the shortening of the radiative lifetime of the emitter via the Purcell effect does indeed restore photon indistinguishability, while at the same time we demonstrate the resonant character of the Purcell effect.

In a second-order interference experiment, when two photons arrive with a relative time delay of  $\tau$  on the two input ports of a beam splitter with (intensity) reflectivity  $R$ , transmission  $T$ , and no losses ( $R+T=1$ ), the probability that the two photons exit through two different output ports (normalized to the value of 1 for the case of random events) is given by the second-order correlation function defined as

$$g^{(2)}(\tau) = \frac{\langle \hat{E}_1^-(t) \hat{E}_2^-(t+\tau) \hat{E}_2^+(t+\tau) \hat{E}_1^+(t) \rangle}{\langle \hat{E}_1^-(t) \hat{E}_1^+(t) \rangle \langle \hat{E}_2^-(t+\tau) \hat{E}_2^+(t+\tau) \rangle}, \quad (4)$$

where  $\hat{E}_i^\pm(t)$  are the electric-field operators at the  $i$ th output port of the beam splitter, while the angular brackets denote

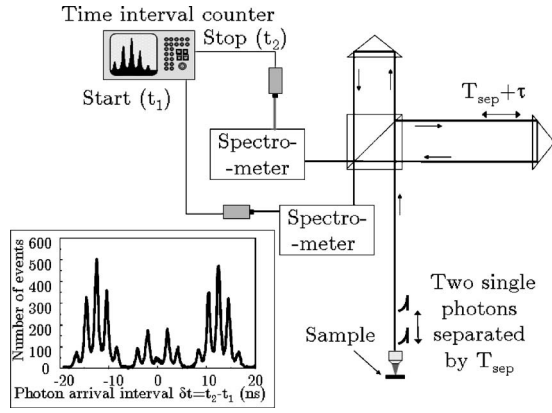


FIG. 1. Experimental setup used to observe quantum interference with two consecutive single photons. Inset: Histogram of the time intervals between “start” and “stop” detection events; the small area of the central peak (ideally zero) indicates that the two photons both go to the same output, since the probability of photodetection coincidence vanishes.

quantum-mechanical averaging with respect to the state of the electromagnetic field. For the case of photons emitted by a quantum dot in the presence of dephasing, the second-order correlation function can be evaluated as<sup>11</sup>

$$g^{(2)}(\tau) = 1 - \frac{2RT}{1 - 2RT} \left[ \frac{T_2}{2T_1} e^{-2|\tau|/T_2} + \frac{T_2^*}{2T_1} (e^{-|\tau|/T_1} - e^{-2|\tau|/T_2}) \right]. \quad (5)$$

Thus, the probability that two photons arriving simultaneously ( $\tau=0$ ) exit through different output ports, relative to the probability of random events, is given by

$$g^{(2)}(0) = 1 - \frac{2RT}{1 - 2RT} \times \frac{T_2}{2T_1} \quad (6)$$

and can be taken as a measure of the “degree of distinguishability” of the two photons, assuming that there is perfect polarization, spatial and spectral overlap of the two photons, and that there is no time jitter in the start of each photon emission.

The microcavities used in this series of experiments are 400-nm-diam micropillars, fabricated by *e*-beam lithography and reactive ion etching from a GaAs/AlAs-layered planar structure grown by molecular-beam epitaxy. These micropillars display a single mode centered around 910 nm with a *Q* factor of approximately 1500. The 300-nm-thick GaAs cavity spacer bounded by two Bragg mirrors contains in its center a single layer of InAs quantum dots whose photoluminescence is centered around 950 nm. This large detuning between the cavity mode and the spectral distribution of the quantum dots is introduced on purpose so as to reduce the number of quantum dots coupled to the mode. Thus, most of the micropillars fabricated in this way contain only one or two dots in resonance with the cavity mode.

In our experimental setup, presented on Fig. 1, the sample is mounted in a He-flow cryostat with variable temperature

control. The micropillar is excited from a steep angle by a pair of laser pulses separated by  $T_{sep}=2.2$  ns and resonant with an absorption of the quantum dot (typically 30–40 meV above the exciton transition energy, thus corresponding to an excited state of the exciton). The two-pulse excitation sequence is repeated with a period of 12.2 ns. Upon each excitation event, the dot emits only one photon in the microcavity at the exciton wavelength. The emitted photons exit the microcavity, are collected by a microscope objective (NA=0.4), and are sent to the two arms of an unbalanced Michelson interferometer which introduces a propagation delay between the short and long paths of  $T_{sep} + \tau$ . In order to select radiation only at the exciton wavelength, two 0.32-m monochromators tuned to that wavelength are placed one on each of the two output ports  $i=1, 2$  of the interferometer. The output of each monochromator is then fed to a single-photon silicon avalanche photodiode, connected, respectively, to the start ( $t_1$ ) and stop ( $t_2$ ) inputs of a time-interval counter. This counter builds a histogram of the time intervals  $\delta t=t_2-t_1$  between start and stop detection events.

Figure 1 presents such a histogram for  $\tau=0$ . It displays a series of five-peak clusters separated by 12.2 ns, the period of the repetition cycle. Looking at the central cluster, the central peak ( $\delta t=0$ ) corresponds to the situation in which the first photon emitted by the quantum dot follows the long arm of the interferometer, thus being delayed to arrive at the same time as the second photon which follows the short arm; for the peaks at  $\delta t=\pm T_{sep}$ , both photons pass through the same arm; finally, for the peaks at  $\delta t=\pm 2T_{sep}$ , the first photon enters the short arm of the interferometer while the second photon enters the long arm. At each delay setting  $\tau$  of the Michelson interferometer, the value of the second-order correlation function can be deduced from the area of the central peak of the histogram ( $\delta t=0$ ) appropriately normalized as

$$g^{(2)}(\tau) = \frac{2 * A_{\tau}(0)}{A_{\tau}(T_{sep}) + A_{\tau}(-T_{sep})}, \quad (7)$$

where  $A_{\tau}(\delta t)$  is the area of the peak at time interval  $\delta t$  on the histogram, with the Michelson interferometer set at a delay of  $T_{sep} + \tau$ . Note that for nonzero delays,  $\tau \neq 0$ , the central peak at  $\delta t=0$  divides into two peaks separated by  $2\tau$ , however usually unresolved by our system which has a resolution of 400 ps.

Two sets of experiments were carried out: In the first experiment, the sample was maintained at 4 K and a micropillar with a resonant quantum dot was chosen, so as to maximize the degree of indistinguishability of the emitted photons. The dependence of the second-order correlation function on the time delay  $g^{(2)}(\tau)$  is shown in Fig. 2. The experimental data is fitted by Eq. (5), with  $R=0.55$  and  $T=0.45$ , assuming perfect spatial, spectral, and polarization overlap. The emission lifetime  $T_1$  and the coherence time  $T_2$  are used as fitting parameters, and a good fit is obtained with  $T_1=110$  ps and  $T_2=165$  ps. In order to check the values obtained by the fit, the lifetime  $T_1$  is measured independently using a streak-camera system with a temporal resolution of 5 ps, while the coherence time  $T_2$  is measured by balancing the Michelson interferometer (i.e., removing the extra delay

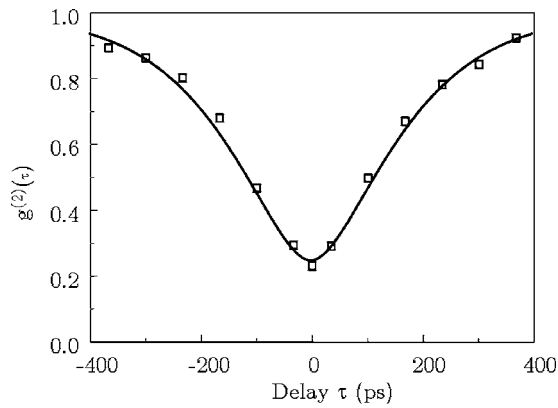


FIG. 2. Second-order correlation function for the photoluminescence of a quantum dot ( $T \approx 4$  K) excited at 888 nm and emitting, respectively, at 916 nm. The solid line is a fit to Eq. (5), with  $T_1 = 110$  ps and  $T_2 = 165$  ps.

$T_{sep}$ ) and measuring the first-order interference fringe contrast as a function of the delay  $\tau$ . The experimentally measured values of  $T_1 = 105$  ps and  $T_2 = 170$  ps are very close to the values obtained by the fit, underscoring the good agreement between theory and experiments. It should be noted that no corrections need be applied to the experimental  $g^{(2)}(\tau)$  values obtained from Eq. (7) and shown in Fig. 2, to account for experimental imperfections, such as misalignments, deduced from the visibility of first-order fringes: second-order interference is insensitive to this apparent reduction of visibility. Contrary to previous measurements performed on single dots,<sup>7</sup> our raw experimental results fit perfectly with theoretical expectations<sup>11</sup>: the  $g^{(2)}$  curve dips down to  $1 - T_2/2T_1$ , as predicted by theory and goes up to the value of 1 essentially exponentially with a time constant close to  $T_1$ , as expected for purely indistinguishable single photons. The radiative lifetime obtained in this experiment, when compared with the typical lifetime of our quantum dots in the absence of a microcavity (of the order of 1.5 ns at 4 K, measured directly by time-resolved experiments<sup>12</sup>) indicates an enhancement of spontaneous emission (Purcell factor) of  $F_p = 1500/110 \approx 14$ . The pure dephasing time of  $T_2^* = 660$  ps, obtained from Eq. (1), is similar to that reported by Borri *et al.*<sup>13</sup> and the coherence factor (or degree of indistinguishability) for the photon wave packets reaches  $T_2/2T_1 = 0.75$ , the highest raw value reported up to now. This coherence factor is limited essentially by the relatively modest Purcell factor of 14 that was reached in this experiment.

In the second set of experiments, the temperature of the sample was varied in the same run at 11 different temperatures ranging from 4 to 46 K. At each temperature, three types of measurements were performed: (1) the full second-order correlation function  $g^{(2)}(\tau)$  to extract the corresponding values for  $T_1, T_2$ , and  $T_2^*$ ; (2) the contrast of the first-order interference fringes to provide an independent measure of  $T_2$ ; and (3) the relative detuning of the quantum dot emission with respect to the microcavity resonance.

As temperature increases, the dephasing time  $T_2^*$  decreases monotonically due to the increase of the thermal phonon population,<sup>14</sup> dropping from 420 ps at 4 K to only 36 ps at 46 K, as can be seen in Fig. 3. At the same time, the change

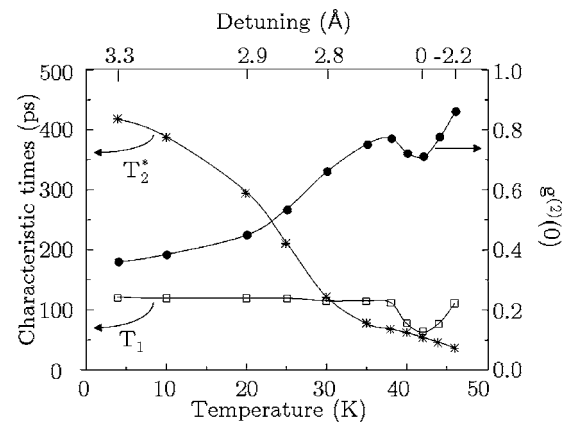


FIG. 3. Characteristic time for pure dephasing  $T_2^*$  (stars), radiative lifetime  $T_1$  (squares), and second-order correlation function at zero delay  $g^{(2)}(0)$  (circles) of the emitting exciton state as a function of temperature and of cavity-exciton detuning.

in temperature causes a shift in the quantum dot exciton energy and to a lesser extent to the frequency of the microcavity, thus modifying the dot-cavity detuning and spanning approximately 0.55 nm. This changes the resonance conditions and, through the Purcell effect, it modifies the radiative lifetime of the quantum dot. As can be seen in Fig. 4, the variation of the lifetime as a function of detuning, expected from Eqs. (2) and (3), follows the spectral profile of the cavity mode, thus underscoring the resonant character of the Purcell effect. In the detuning range examined in these experiments,  $T_1$  drops from 117 ps (corresponding to  $F_p \approx 13$ ) at  $\Delta\lambda = 0.33$  nm to 65 ps ( $F_p \approx 23$ ) at resonance and increases back to 110 ps at  $\Delta\lambda = -0.22$  nm, indicating that the detuning span is consistent with the  $Q$  factor of 1500.

The strong decrease of the pure dephasing time with temperature degrades the indistinguishability of the photons. However, the enhancement of the spontaneous emission lifetime by the Purcell effect can partially restore the indistinguishability of the photons and the visibility of the second-order interference. This can be seen in Fig. 3, which presents the second-order correlation function at zero delay  $g^{(2)}(0)$  as a function of temperature. As temperature increases, the visibility of the second-order interference [corresponding to de-

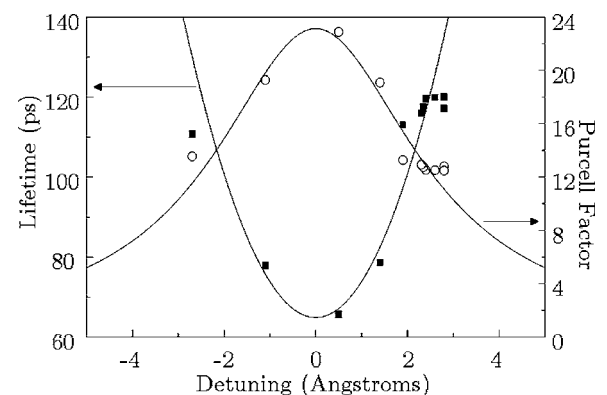


FIG. 4. Radiative lifetime  $T_1$  and Purcell factor  $F_p$  as a function of the exciton-cavity detuning  $\Delta\lambda$ , fitted by a Lorentzian.

viation of  $g^{(2)}(0)$  from the ideal value of 0] is degraded, essentially because of the increased dephasing. However, at the temperature of 38 K, the second-order visibility starts improving, reaching a local minimum at 42 K, where the quantum dot is on resonance with the cavity mode. This demonstrates that the shortening of the radiative lifetime associated with the resonant condition of the Purcell effect improves the coherence factor of the photons and restores their indistinguishability.

In conclusion, the visibility of a second-order interference experiment can serve as a measure of the degree of indistinguishability of the two photons being mixed at the beam splitter. The presence of dephasing processes, which become stronger with temperature, degrades the indistinguishability of the photons. Nevertheless, implementation of the Purcell effect in a microcavity to shorten the radiative lifetime of a

quantum dot can overcome the dephasing of the emitting state, improve the coherence factor of the photons, and restore their indistinguishability. Second-order interference was thus observed for temperatures up to 46 K. The resonant character of the Purcell effect was clearly demonstrated in these experiments, where a spontaneous emission enhancement factor of 23 was achieved at resonance. Cavities with a higher quality factor should permit restoration of photon indistinguishability and observation of second-order interference at higher temperatures, and the attainment of visibilities close to 1 at low temperatures, an important requirement for using second-order interference in cascaded quantum logic gates.

This work was supported in part by a contract from the French Ministry of Research (“POLQUA”).

<sup>1</sup>C. K. Hong, Z. Y. Ou, and L. Mandel, *Phys. Rev. Lett.* **59**, 2044 (1987).

<sup>2</sup>J. G. Rarity and P. R. Tapster, *Phys. Rev. A* **41**, 5139 (1990).

<sup>3</sup>A. M. Steinberg, P. G. Kwiat, and R. Y. Chiao, *Phys. Rev. Lett.* **71**, 708 (1993).

<sup>4</sup>E. Knill, R. Laflamme, and G. J. Milburn, *Nature (London)* **409**, 46 (2001).

<sup>5</sup>H. de Riedmatten, I. Marcikic, W. Tittel, H. Zbinden, and N. Gisin, *Phys. Rev. A* **67**, 022301 (2003).

<sup>6</sup>Th. Legero, T. Wilk, M. Hennrich, G. Rempe, and A. Kuhn, *Phys. Rev. Lett.* **93**, 070503 (2004).

<sup>7</sup>C. Santori, D. Fattal, J. Vuckovic, G. S. Solomon, and Y. Yamamoto, *Nature (London)* **419**, 594 (2002).

<sup>8</sup>J. M. Gérard, B. Sermage, B. Gayral, B. Legrand, E. Costard, and

V. Thierry-Mieg, *Phys. Rev. Lett.* **81**, 1110 (1998).

<sup>9</sup>E. M. Purcell, *Phys. Rev.* **69**, 681 (1946).

<sup>10</sup>D. Fattal, K. Inoue, J. Vuckovic, C. Santori, G. S. Solomon, and Y. Yamamoto, *Phys. Rev. Lett.* **92**, 037903 (2004).

<sup>11</sup>J. Bylander, I. Robert-Philip, and I. Abram, *Eur. Phys. J. D* **22**, 295 (2003).

<sup>12</sup>I. Robert, E. Moreau, J. M. Gérard, and I. Abram, *J. Lumin.* **94–95**, 797 (2001).

<sup>13</sup>P. Borri, W. Langbein, S. Schneider, U. Woggon, R. L. Sellin, D. Ouyang, and D. Bimberg, *Phys. Rev. Lett.* **87**, 157401 (2001).

<sup>14</sup>C. Kammerer, C. Voisin, G. Cassabois, C. Delalande, Ph. Rousignol, F. Klopff, J. P. Reithmaier, A. Forchel, and J. M. Gérard, *Phys. Rev. B* **66**, 041306(R) (2002).